Assembly of small molecule surfactants at highly dynamic air-water interfaces

Omar T. Mansour[a], Beatrice Cattoz[a], Manon Beaube[a], Morganne Montagnon[a], Richard K. Heenan[b], Ralf Schweins[c], Marie-Sousai Appavou[d] and Peter C. Griffiths[a,*]

a. Faculty of Engineering and Science, University of Greenwich, Medway Campus, Central Avenue, Chatham Maritime, Kent, ME4 4TB, UK
b. Science and Technology Facilities Council, ISIS facility, Rutherford Appleton Laboratory, Didcot, Oxfordshire, OX11 0QX, UK
c. Institut Laue Langevin, ILL, 6 rue Jules Horowitz, 38000 Grenoble, France
d. Forschungszentrum Julich, JCNS at FRM II, Lichtenbergstrasse 1, 85747, Garching, Germany

* *corresponding author: p.griffiths@greenwich.ac.uk*

Abstract

Small-angle neutron scattering has been used to probe the interfacial structure of foams stabilised by small molecule surfactants at concentrations well below their critical micelle concentration. The data for wet foams showed a pronounced Q^{-4} dependence at low Q and noticeable inflexions over the mid Q range. These features were found to be dependent on the surfactant structure (mainly the alkyl chain length) with various inflexions across the measured Q range as a function of the chain length but independent of factors such as concentration and foam age/height. By contrast, foam stability (for C < CMC) was significantly different at this experimental range. Drained foams showed different yet equally characteristic features, including additional peaks attributed to the formation of classical micellar structures. Together, these features suggest the dynamic air-water interface is not as simple as often depicted, indeed the data have been successfully described by a model consisting paracrystalline stacks (multilayer) of adsorbed surfactant layers; a structure that we believe is induced by the dynamic nature of the air-water interface in a foam.

Introduction

Foams are systems comprising concentrated dispersions of gas bubbles in a continuous aqueous phase, and are widely encountered as precursors in a number of applications, *e.g.* medical,[1,2] insulation materials,[3] cosmetic[4] and firefighting.[5] There has also been a recent interest in these systems for their applications in food industries.[6,7] For the majority of foams, the aqueous phase contains surfactants or proteins, which act as stabilisers.

Physicochemical properties of the solutions formed the foams such as ionic strength, pH, and temperature significantly affect the interfacial behaviour of the foaming agents or stabilisers (surfactants). It is well established that surfactants and their blends are of crucial importance to foam formulations.[8–10] In the absence of surfactants, a foam will catastrophically coalesce and collapse,[11,12] whereas in their presence, the interface is efficiently stabilised by (monomer) adsorption at the air-water interface as evidenced by changes to the surface tension, surface shear viscosity and surface elasticity.[13,14]

Recently, it has become clear that surfactant stabilised air-water interfaces are not as simple as initially thought. Thomas *et al*. have extensively reviewed the formation of multilayer surfactant structures at the air-water interface using tensiometry and neutron reflectivity (NR). Contrary to the classical monolayer picture, the surfactants (as dioctyl sulfosuccinate sodium (AOT), didoceyldimethylammonium bromide (DDAB), sodium laureth sulfate (SLES)), investigated presented multilayering phenomenon over a wide range of systems, with and without additives.[15]

Above some (bulk) critical micelle concentration (CMC), there are substantial changes in several characteristics of the properties of the solution.[16–19] A similar situation exists in foams. Petkova *et al.*[12] have determined a “transitional concentration” above which, foams were found to be stable, these concentrations being 10-30 times **below** the CMC for the surfactants studied (sodium dodecylsulfate, dodecyltrimethylammonium bromide and Brij 35). This indicates that the surfactant at the interface has a very different character than the surfactant in the bulk phase.

Partially hydrophobic colloidal silica particles have also been shown to adsorb at the air-water interface where it was found that these particles form a “colloidal armour” at the interface that stabilises the foams for durations up to months.[20,21] Most studies

have necessarily focused on the process of foaming and foam stabilization using traditional measurements (foam half-life, bubble size measurement, *etc*.), but far fewer studies have investigated directly the complex interfacial structure formed by these molecules, within macroscopic foam and/or single foam films.

Neutron and X-ray reflectivity have been used extensively to quantify the gas-liquid interface, but on planar interfaces, and not under dynamic conditions relevant to the foam.[22–28] There also have been a number of small angle scattering studies on foams, [29–34] illustrating the viability of the technique, but the conclusions have been largely qualitative and are yet to improve the understanding of the assembly of stabiliser at the air-water interface.

Using small-angle neutron scattering (SANS), Axelos *et al.*[30] studied a series of wet and dry foams generated with sodium dodecylsulfate ($C_{12}SO_4Na$, SDS) with varying concentrations. Under steady state foaming conditions (the so-called “wet foam”), a pronounced Q^{-4} dependence was observed with a number of peaks - “bumps” - varying in shape and position, depending on the surfactant concentration. Specifically, SANS from wet foams stabilised by SDS at 3 g/L shows a pronounced Q dependence at low Q, but no peaks were observed in the data. At higher SDS concentrations, 25 g/L, a single peak at high Q was observed, similar to the q value obtained from SDS in bulk solution *i.e*. micelles were present in the liquid in the walls. Upon drainage (“dry foams”), peaks were also observed at intermediate Q ($Q \approx 0.03$ Å^{-1}) for different SDS concentrations, attributed to the film thickness.

Ropers *et al.*[31] along with the previous authors studied hexadecyltrimethylammonium bromide (CTAB), and polysaccharide/CTAB complex stabilised free draining foams also by SANS. A different approach towards data interpretation was used and the data were analysed from both scattering and reflectivity points of view. They concluded that the polysaccharide addition yields a shift in the peak position towards lower Q values and that the peak was attributed to the film thickness. It was also postulated that this shift is insensitive to the drainage duration and that the emergence of yet another peak was the result of a thicker liquid film.

Micheau *et al.*[34] have investigated foams from the pH sensitive nonaoxyethylene oleylether carboxylic acid, where their modelling and analysis was shaped by the work of Axelos and co-workers. Similar SANS data features were observed and the authors concluded that the oscillations in the data originate from the reflectivity of neutrons

within thin liquid films within the foam. The thickness of these liquid films was found to be sensitive to pH and surface charge.

However, it was not entirely clear how the contribution of micelles and lamellar structures on the observed scattering was taken into account. The concentration of the surfactant in those samples was well above the CMC, and as such, complex structures (micelles and foam-induced surfactant lamellae) are expected to be present. These structures would give rise to significant scattering in those *Q* regions under discussion. Similarly, Axelos *et al*. previously correlated the observed scattering features with micelles present in the liquid in the walls of wet foams stabilised by SDS above the CMC.

There is still a debate as to whether these inflexions arise from the film thickness of the bubbles (160-180 Å) or a surfactant structure at the interface. Fameau *et al.*[35] have studied a series of foams stabilised by thermo-sensitive fatty acids (12-hydroxy-stearic acid, 12-HSA) using SANS amongst other techniques, where they compared scattering data from bulk solution and the foams (wet and dry). A series of Bragg peaks were observed at different *Q* positions, which they attributed to the presence of multilamellar tubular arrangement of the fatty acid bilayers in the foam. They have also studied these systems at different H_2O/D_2O compositions from both scattering and reflectivity points of view, utilising contrast variation. It was found that for a reflectivity experiment, as the H_2O content increases, the position of the peaks shift, and for a SANS experiment, when the H_2O content increases, no shift in the peaks were observed but only a decrease in the scattering intensity was recorded. Based on these findings, the authors have demonstrated that the SANS signal originates from tubes present in the liquid foam and eliminated the possibility of the signal originating from the reflectivity of neutrons at the air-water interface.

Fameau *et al.*[28] have also studied the interfacial structure of the ethanolamine salt of the same thermo-sensitive fatty acid mentioned above in solution, using tensiometry and NR. The NR data showed a series of fringes which the authors related to the presence of a large layer of fatty acid materials at the air-water interface. This layer was found to be of thickness of ≈ 300 Å. The NR data was modelled according to different possible arrangements of the fatty acid layer, and it was concluded that the presence of the fringes in the data is due to the multilamellar tubes from the fatty acid being adsorbed at the air-water interface.

NR was deployed by Ederth *et al.*[36] to monitor the structure of foam films from AOT. The authors observed weak Bragg peaks, which have been attributed to a lamellar structure of AOT bilayers in the foam films. This weak intensity profile of the Bragg peaks has been related to the small number of layers of AOT that contributes to the scattering in the films, films inhomogeneities and the presence of other structures such as disk like micelles or discontinuous bilayers.

Foams stabilised by SDS in the presence of high concentrations of sodium and potassium chloride; NaCl and KCl, were studied by Zhang *et al.*[32] The high salt concentrations induced the precipitation of the SDS at the surface of the bubbles leading to the formation of ultrastable foams. This was attributed to the stopping of the ageing of the foam due to the presence of the surfactant crystals between the bubbles. The presence of these crystals was later confirmed by SANS, where two peaks arising from the crystals were observed at high *Q*. It was concluded that these two peaks are related to the interplanar distance present in the SDS lamellar structure.

Solution and foam structures from the non-ionic surfactant polyglycerol ester (PGE) were studied by Curschellas *et al.*[33] using a combined approach of electron microscopy, NR and SANS. The SANS measurements have allowed the authors to draw a comparison between the scattering behaviour of the bulk solution and its corresponding foam. In solution, the SANS data revealed that the PGE forms multilamellar structures, confirmed by the presence of Bragg peaks. Whilst in the foam case, there was no significant difference from the scattering of the bulk solution. This was concluded to be a result of the scattering from the entrapped bulk solution, which in return, helped produce more stable foams as the vesicles presence blocked the plateau borders and eventually had an effect on the drainage.

Hurcom *et al.*[37] have previously successfully used SANS to study air-in-water foams stabilised by a series of Pluronic block copolymers at different concentrations below and above the CMC. Similar SANS features were observed for all the foams for all systems. The data below the CMC was interpreted and modelled as a paracrystalline stack of polymeric surfactant lamellae at the air-water interface. The thickness of these layers was found to be dependent on the EO and PO block characteristics and the overall molecular weight of the polymer.

Against this backdrop, the hypothesis being advanced here follows our previous work (*Soft Matter,* 2014, 10, 3003-3008), where SANS was used to demonstrate the presence of a surfactant multilayer structure at the foam air-water interface. The current experiments here have been designed to study the interfacial structure of wet foams (continuously generated) stabilised by a range of small amphiphilic molecules; alkyl sulfates ($C_nH_{2n+1}SO_4Na$) and alkyl bromides ($C_nH_{2n+1}TABr$) at concentrations well below the established bulk surfactant CMCs, as measured by surface tension, Figure S.1 and S.2 (Table S.1 and S.2 in very good agreement with literature[38,39]). Hence, this study is differentiated from others in the sense that since it is assumed that the surfactant concentrations within the water film are too dilute to contain any conventional micelles.

Experimental

Materials

Homologous series of ionic surfactants were used as received, as listed in Tables S.1 and S.2. Solutions for SANS experiments were prepared in deuterated water (99.9%, Sigma Aldrich).

Methods

Tensiometry*.* Surface tension measurements were carried out using a maximum bubble pressure tensiometer (SITA science on-line t60, Germany), calibrated by reference to de-ionized water. Surface tension was recorded at a bubble lifetime of 10 seconds. All measurements were performed at 25 ± 1°C.

Foam stability. Foam stability measurements were carried out in a graduated glass column, 45 cm in height and 20 mm in diameter. The column was fitted was a porous frit disk (porosity of 2 µm) placed at the bottom of the column. The airflow was controlled via a flow meter (0-0.5L/min). Nitrogen gas was passed through the sample (2.5 cm^3 of the surfactant solution placed in the bottom of the column) at a constant flow rate of 0.04 L/min and 0.4 bar pressure. Foam with a standard height of 15 cm was generated, after which the gas flow was turned off and the foam was allowed to drain. The half-life taken by the foam to lose half of its original height recorded. All measurements were recorded twice; new aliquots of surfactant solution were used for

each foam test and the column was washed with deionised water and dried between each test to ensure reproducibility.

Small-angle neutron scattering (SANS). As wet foams were of main interest in this work, there was a continuous bubbling through the surfactant solution, which produces constantly regenerated foam. As such, the bubbles appear spherical and thick lamella walls separate them (ESI). All experiments were performed at room temperature.

SANS experiments were performed on either (i) the time of flight (a) *LOQ* and (b) *SANS2d* diffractometers at the ISIS pulsed spallation neutron source, Rutherford Appleton Laboratory, Didcot, UK. A range defined by $Q = (4\pi/\lambda) \sin(\theta/2)$ between 0.009 and ≥ 0.5 $Å^{-1}$ (*LOQ*) and 0.005 and ≥ 0.3 $Å^{-1}$ (*SANS2d*) was obtained by using neutron wavelengths (λ) spanning 2.2 to 10.0 Å with a fixed detector distance of 4 m (*LOQ*) and 1.75 to 16.5 Å with a fixed detector distance of 4 m (*SANS2d*). (ii) steady-state reactor sources at (a) *D11* diffractometer at the ILL, Grenoble where a *Q* range is selected by choosing three instrument settings at a constant neutron wavelength (λ) of 8 Å (ILL) with a sample detector distance of 1.2, 8 and 39 m, and (b) *KWS-1* diffractometer at the Jülich Centre for Neutron Science at FRM II, Garching, using three detector distances (2, 8 and 20 m) and a neutron wavelength of 5 Å.

Experimental measurement times were around 5 minutes (*LOQ* and *SANS2d*) and between 10-15 minutes *(MLZ* and *ILL*, longer as three detector distances were used with no hysteresis). All scattering data were (a) normalized for the sample transmission, (b) background corrected using the empty foam cell and, (c) corrected for the linearity and efficiency of the detector response using the instrument specific software package and the scattering from a polystyrene blend taped to the front of the foam cell, Figure 1.

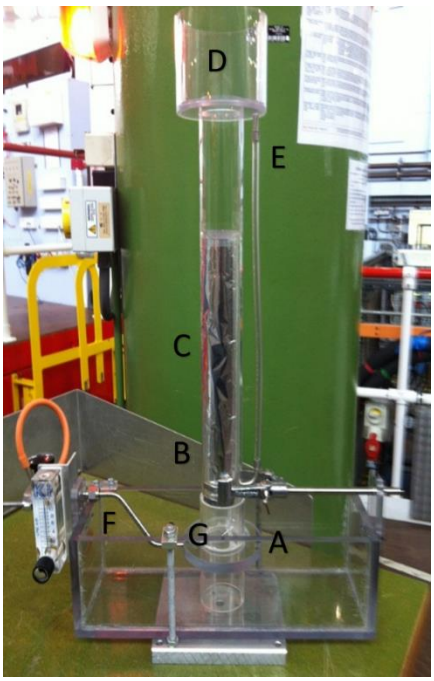

Figure 1. SANS sample environment for studying foams. The foam was generated by pushing nitrogen gas through a 20 μm frit (A) at the base of a Perspex column (height of 25 cm, diameter of 4.6 cm), which contains approximately 50 mL of the surfactant solution. A 2 cm wide groove has been removed and covered with aluminium foil to allow the neutrons to cross the sample. The neutron beam impinges on the aluminium foil between (B) and (C) behind which the Perspex has been partially removed. For stable foams, the reservoir (D) collects the foam sample and returns it to the base via the plastic tube at (E). The cell is also be equipped with a controlled heating set up (heating jacket) at (F) and (G); however, it was not used in this study to actively control the temperature. [37]

Results and Discussion

The bulk of this study presents the scattering from foams that are continuously generated; foams pass into the neutron beam within seconds of creation. These we call “wet foams”. One can also look at draining foams by removing the gas flow and observing the foam within the beam at different levels of drainage (or time and height). These we call “draining” or “dry foams”, but such foams are of secondary importance in this paper but presented to reinforce the interpretation of the scattering from the wet foams. We are also particularly interested in solutions well-below the CMC, but again, we present data from C> CMC to highlight similarities and therefore differences with the C < CMC data.

SANS from wet foams for C > and C < CMC; an empirical comparison

The scattering in these systems may arise from (a) any structure normal to the air-water interface, which would follow an approximate Q^{-4} dependence given that these interfaces are not perfectly flat, (b) any in plane structure normal to the interface, (c) fluctuations in the composition of the interfaces parallel to the beam, (d) structures that would be present in the liquid junctions between the bubbles, this may resemble the ‘bulk solutions’ at appropriate concentration, and (e) in the aged polyhedral foams, the long almost cylindrical regions at the junction of bubbles associated with the plateau borders.

Representative data are presented in Figure 2a (recorded on *D11*) from continuously generated foams from a series of small molecule surfactants (SMS). The data shows a number of features; the pronounced Q^{-4} dependence at low Q, characteristic of the Porod scattering from a smooth surface with a large radius. Over the mid Q range, there are the noticeable inflexions or “bumps” around 0.038 $Å^{-1}$ for $C_{12}SO_4Na$ corresponding to *d-spacing* ($2\pi/Q_{peak}$) of 165 Å, whilst for the $C_{12}TAB$ case, the inflexion occurs at 0.037 $Å^{-1}$ corresponding to a spacing of 170 Å.

Given that these concentrations are below their CMC, no (solution-like) micelles are assumed to be present. Therefore, the observed peaks do not arise from the micellar form factor $P(Q)$. As justification, the scattering from foams stabilised by $C_{12}SO_4Na$ solutions above the CMC (10 mM) is also shown in the inset in Figure 2a, these data are in excellent agreement with Axelos *et al.*[30] *and* Hurcom *et al.*[37], where the maxima at $Q \approx 0.04$ $Å^{-1}$ relates to the micellar scattering from the surfactant micelles in the liquid forming the walls. For $Q > 0.2$ $Å^{-1}$, the data decay into an incoherent background

scattering that varies from one system to another depending on the amount of the sample in the beam. It is worth mentioning that the SANS data were obtained reproducibly for foams from all the four different diffractometers used in this study, and were all in excellent agreement in terms of features and peak positions (exemplary data from C_{12}TAB foams is presented in Figure S.3).

A simple approach to adopt towards the **visualization** of data with a strong Q^{-n} (where n = 4 ± 0.05) is Porod plots; $Q^n I(Q)$ *vs* Q. This entirely removes the Q^{-n} dependence and emphasises any other features observed in the data, *i.e.* the peaks, and clearly allows for the comparison with solution scattering, Figure 2b.

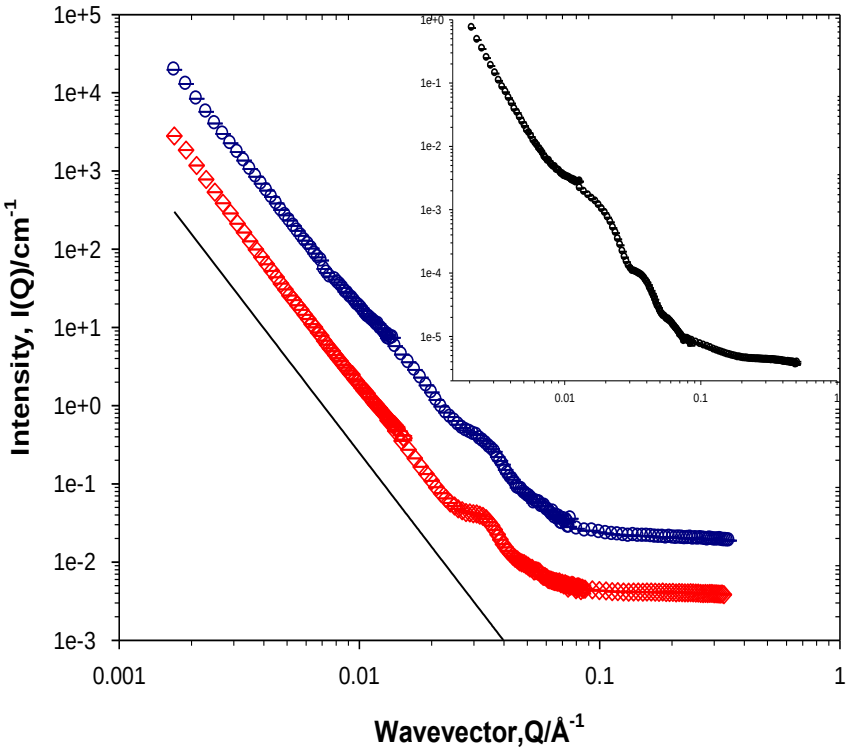

Figure 2a. SANS from foams stabilised with 4 mM $C_{12}SO_4Na$, (circles) and 7 mM C_{12}TAB (diamonds) in D_2O. Typical Q^{-4} dependence is presented as a solid line. Data have been offset for clarity. Inset presents the scattering from foams stabilised by 10 mM $C_{12}SO_4Na$ in D_2O. Data recorded on *D11*.

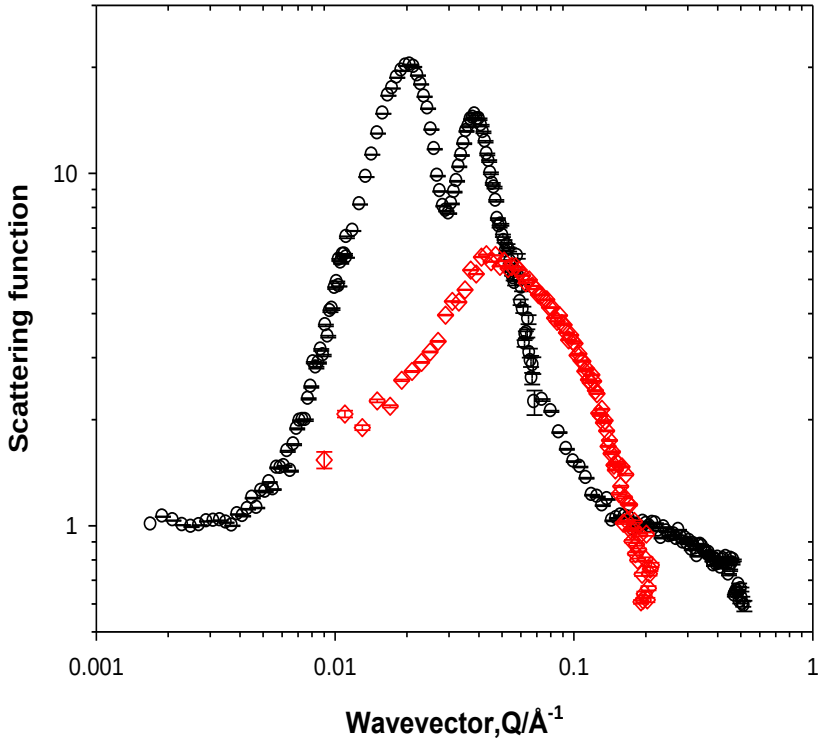

Figure 2b. Porod analysis, I(*Q*)Q*^{n} (circles) from foams stabilised by SDS, C > CMC (*D11*) and I(*Q*)/cm^{-1} (diamonds) from SDS, C > CMC in bulk solution (*LOQ*).**

On can clearly deduce that the $Q \approx 0.04$ Å^{-1} peak is related to the micelle form factor *P(Q)*. The $Q \approx 0.015$ Å^{-1} peak is not and could be attributed to the presence of a lamellar ordering of the $C_{12}SO_4Na$ between the foam walls, and suggest that the foams induce this surfactant lamellar structure.

Similar observations could be noted from the SANS data from wet foams stabilised by lower $C_{12}SO_4Na$ concentrations. At concentrations as low as 1 mM (significantly below the bulk CMC), the data still shows the pronounced Q^{-n} behaviour along with the peak at mid *Q*. This peak position remains insensitive to the surfactant concentration used to stabilise the foams, Figure 3 (*SANS2d*). This is a very interesting observation, given that the foam stability measurements (Figure S.4) shows a noticeable difference as the surfactant concentration varies from 1 mM to 4 mM. One would expect there has to be some dependence of the rates of the foam coalescence and eventual collapse on the concentration of the surfactant[40], which in turn is expected to vary the film thickness.

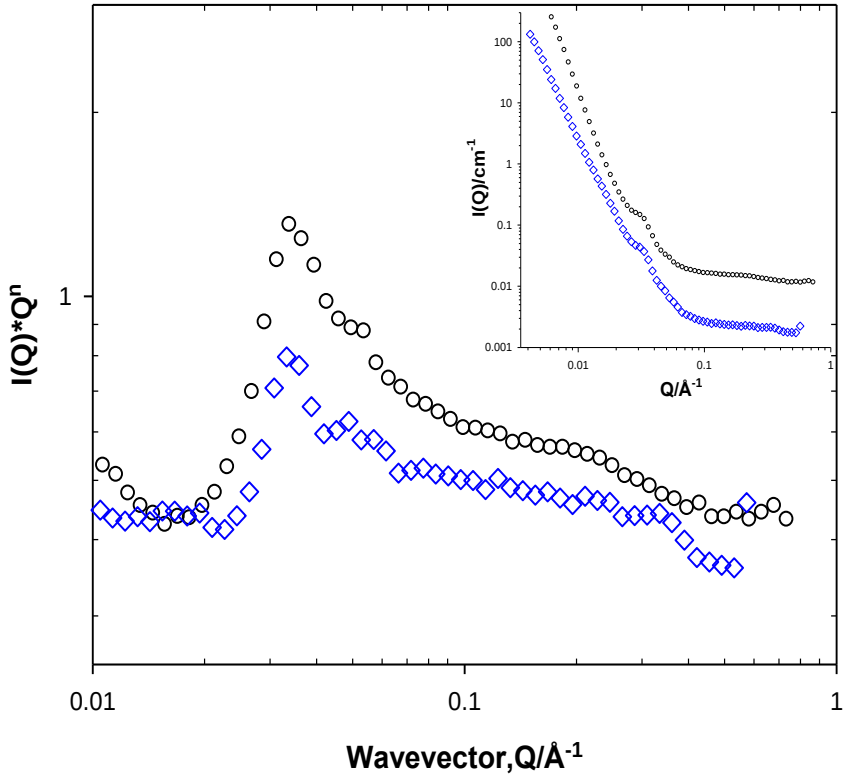

Figure 3. Porod plots from wet foams stabilised with $C_{12}SO_4Na$, at different concentrations, 1 mM (circles) and 4 mM (diamonds) in D_2O. Data have been offset for clarity. Inset presents the I(*Q*) *vs Q* from the same data. Data recorded on *SANS2d*.

This observation can also be extended to the $C_{12}TAB$ case, where upon further decrease in its concentration, 0.25 mM (60 times lower than its CMC), the SANS data for the wet foam, Figure S.7, shows the same features observed at the higher concentration. No significant change in the *q*-value of the peak was observed (0.035 $Å^{-1}$), confirming the assumption that the surfactant concentration in the films was too low to form micelles.

We have also performed neutron scattering experiments to investigate foams stabilised by $C_{12}SO_4Na$ at three different drainage conditions, as shown in Figure 4 (recorded on *D11*). Upon draining, very well defined peaks emerge with maxima at $Q \approx 0.015$ $Å^{-1}$ and 0.042 $Å^{-1}$. Tables 1a and 1b highlight the peak positions obtained by SANS from $C_{12}SO_4Na$ foams and in bulk solution (at different concentrations). The similarities between the *q*-values of the correlation peaks from $C_{12}SO_4Na$ in bulk, Table 1b, and the peaks from 10 mM $C_{12}SO_4Na$ foam strongly suggests that the

scattering is dominated by the solution in the film borders. SANS data from $C_{12}SO_4Na$ in bulk solution have been included in the ESI.

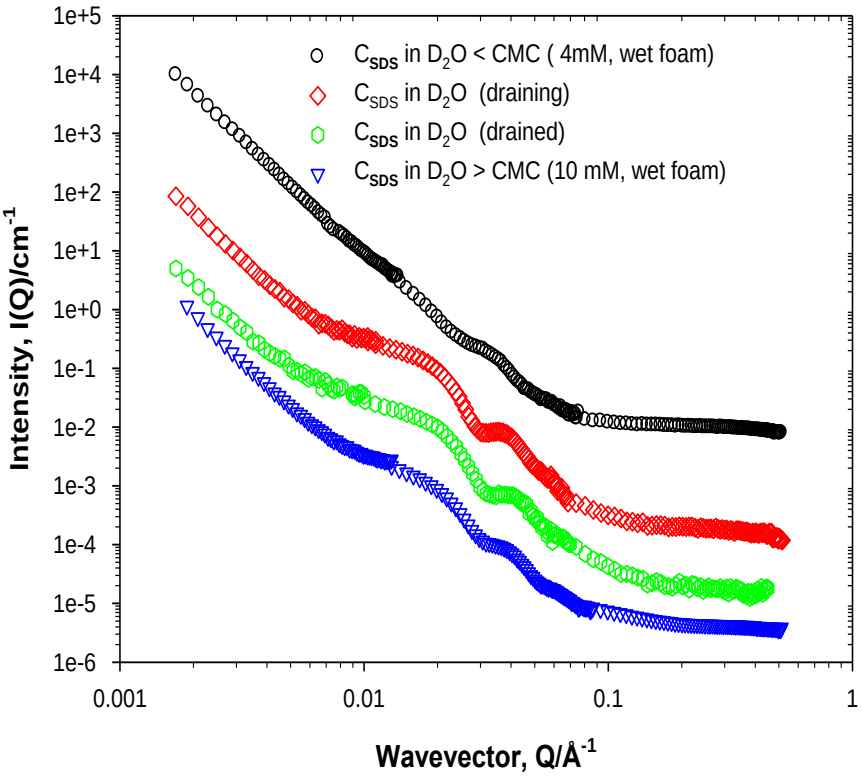

Figure 4. SANS from foams stabilised by $C_{12}SO_4Na$ at different air flow conditions and concentrations. Data have been offset for clarity. Data recorded on *D11*.

System Description	Q_{peak} 1 (Å^{-1})	Q_{peak} 2 (Å^{-1})
4 mM $C_{12}SO_4Na$ (wet foam)	0.038	--
$C_{12}SO_4Na$ – draining	0.016	0.042
$C_{12}SO_4Na$ – drained	0.018	0.045
10 mM $C_{12}SO_4Na$ (wet foam)	0.017	0.044

Table 1a. Positions of first and second maxima in the scattering data from $C_{12}SO_4Na$ foams at different airflow conditions/concentrations.

System Description	Q_{peak} (Å^{-1})
10 mM $C_{12}SO_4Na$	0.040
15 mM $C_{12}SO_4Na$	0.040
20 mM $C_{12}SO_4Na$	0.045
30 mM $C_{12}SO_4Na$	0.047

Table 1b. Correlation peak positions from $C_{12}SO_4Na$ micelles in D_2O at different concentrations.

As the foam drains, we observe significant changes in the scattering patterns, Figure S.8. The emergence of the asymmetric scattering “spikes” on the right is a signature of the transition from spherical (curved bubble walls) to polyhedral bubbles (flat single films[34,41]) as the liquid fraction in the foam decreases.

As the scattering is observed from any appropriately sized structures within the neutron beam, a question arises regarding the relative contributions from interfacial to “bulk” structures. Consider the wet foam as a series of spherical bubbles (radius, R), with film thickness, T, regularly distributed in a cubic array (with cube length 2 (R+T)). As the core of the bubble contains no liquid, the scattering will arise from the structures present at the interfaces and within the “bulk” liquid in the interstitial volumes. It is a relatively simple exercise to calculate the volume of the “halo” of the spherical structure, and the interstitial volumes between the bubbles (the volume of the cube less the volume of the sphere). For millimetre sized bubbles (R = 1.0 x10^{-3} m), with micron thick interfaces (T= 1.0 x 10^{-6} m), over 90% of the total volume in the beam is present in the interstitial zones. Accordingly, for systems above or approaching the CMC, micellar structures will be clearly evident, but for C < CMC, the scattering is necessarily dominated by the interfacial structures.

As a result of these observations, we suggest the inflexions are not related to the total film thickness as suggested by Axelos[30] or most recently Micheau *et al.*[34] as the *d*-spacing values (180 Å ± 5) are too small to represent the thickness of the wet foam films. Similar SANS observations were recorded from lamellar structures present in emulsions stabilised by Pluronic L92,[42] more recently in foams[35] as discussed earlier and in foam thin films by NR.[36]

Given the observation of multi-layers at equilibrium air-water interfaces under certain conditions[15], and against the background just presented, we invoke a model of the air-water interface that embodies multi-layer stacks that captures all of these significant features in the data.

SANS data analysis and modelling C < CMC

The Q^{-n} Porod plots; $Q^n I(Q)$ *vs.* Q representation is useful as it removes the Q^{-n} dependence but does not provide any further detailed structure information. We have therefore employed a model of the air-water interface that comprises multilayers (treated as a paracrystal to account for repeating spacing, Figure 5) of M thin surfactant/water layers (number of stacks), of thickness L, separation D and diffuseness T_i (the variation in interface structure perpendicular to the interface; an ideal interface will have zero diffuseness).[43,44] To this, a Q^n term is added to account for the scattering from the smooth air-water interface. To limit the functionality of the fit, the diffuseness T_i has been constrained to 0.01. In this model, I(Q) = I(Q)*S(Q), where I(Q) is expressed as:

$$I(Q) \longrightarrow N\,(\rho_1 - \rho_3)^2 V^2 \left(\frac{\sin(\frac{QL_1}{2})}{\frac{QL_1}{2}} \right)^2$$

where N is the number of particles per unit volume, cm^{-1}, ρ_1 is the scattering length density (SLD) of the surfactant layer, ρ_3 is the SLD of the solvent, V is the volume of the scatterer and L is the thickness of the surfactant layer. The S(Q) used here is that of a one dimensional paracrystal, equations (9) to (12) in the detailed model description by Kotlarchyk *et al.*[44] The main contributing terms to the S(Q) are M , D as explained earlier and a Gaussian distribution term, $\sigma D/D$. The data are fitted in an I(Q) vs Q representation, and the Q^{-n} component removed post-fitting.

Typical starting values for the heterogeneity of L and D are $\sigma(L)/L$ and $\sigma(D)/D$ = 0.2, though these values have shown to have a negligible effect on the overall quality of the fit within reasonable bounds. The SLDs (contrast) of the various materials is such that in D_2O, the scattering arises equally from the air–D_2O and surfactant–D_2O interfaces, and any further deconvolution of the data is not feasible, at least in these systems.

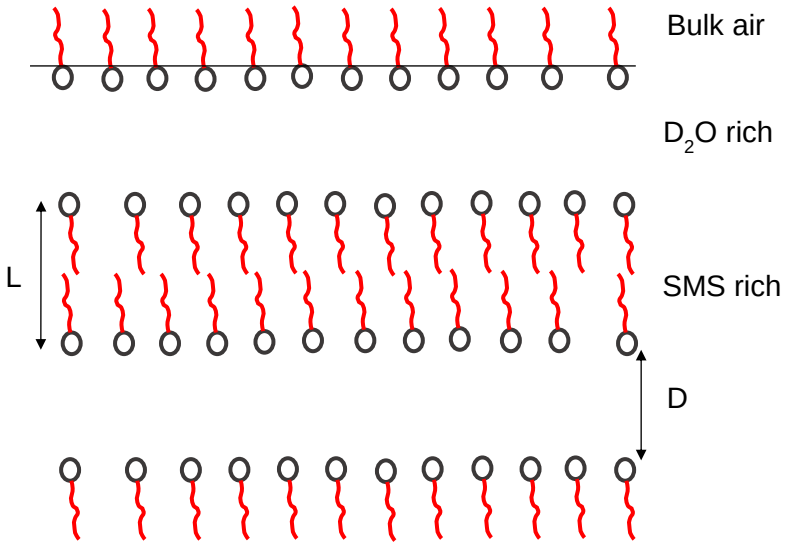

Figure 5. Schematic presentation of the multilayer model of the adsorbed SMS layers at the air-water interface. *L* is the layer thickness and *D* defines the separation. Not to scale.

The thickness *L* (bilayer of surfactant) value was estimated by calculating the critical chain length (Å) of the surfactant (1.5 + (1.26 x N_c) x 2)), where N_c is the number of carbon atoms in the alkyl chain. The value of *M* (number of layers) was found to produce suitable fits at small values (≈5), while larger values did not significantly improve the quality of the fit. No significant difference was observed between the values obtained for *D* from the fitting routine and the *d-spacing* values obtained from the scattering data. Key parameters from the fit are presented in Table 2.

As the SMS hydrophobic chain length increases, subtle changes in the data can be observed. This could be seen in both Figures 6 (alkyl sulfate series) and 7 (alkyl bromide series). As shown in these figures, the multilayer model seems to reproduce the coarse features of the data rather well. An extensive modelling of the data showed that the fit was more sensitive to *L* than *D*, *via* the position of the peak, while the peak width is a compound function of both parameters.

System Description	*L* (Å) ±2	*M*	*D* (Å) ±5
50 mM C_8SO_4Na	26	5	190
16 mM $C_{10}SO_4$ Na	30	5	180
4 mM $C_{12}SO_4Na$	36	4	175
72 mM C_8TAB	26	5	185
29 mM $C_{10}TAB$	30	4	180
7 mM $C_{12}TAB$	40	5	180
1.8 mM $C_{14}TAB$	50	5	177

Table 2. Fit parameters to the scattering from small molecule surfactant stabilised foams at different concentrations below their CMC.

In the ensuing plots, the Q^{-n} term is removed, and subtle deviations from the fitting become more apparent. In Figures 6 and 7, the multilayer model approach reproduces - to a large extent - the position and shape of the main peak in the data, confirming the lengthscales relevant in these systems. In some datasets, the fitting also predicts the presence of the observed secondary features, though those characteristics are captured less well. We interpret these deviations as having their origins in the degree of homogeneity in the multilayer(s).

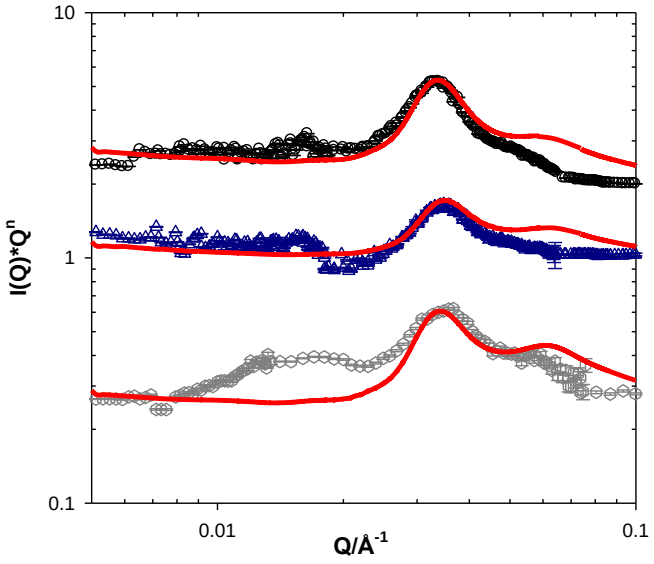

Figure 6. Porod plots from foams stabilised with 50 mM C_8SO_4Na (circles), 16 mM $C_{10}SO_4Na$ (triangles) and 4 mM $C_{12}SO_4Na$ (hexagons). Solid lines are fits to the paracrystalline (multilayer) model described in the text. Data have been offset for clarity. Data recorded on *D11*.

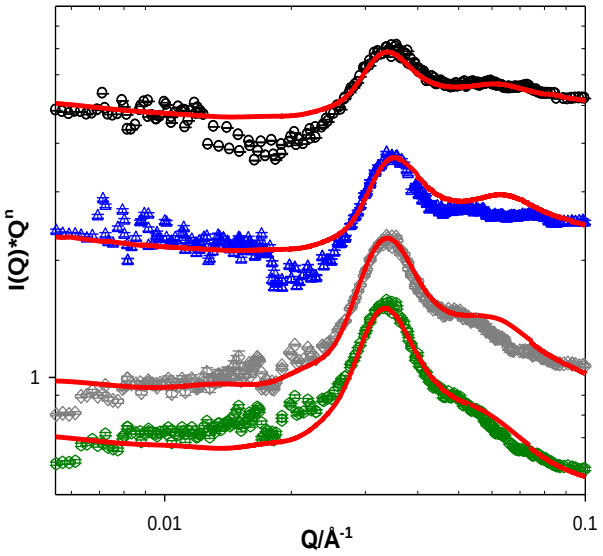

Figure 7. Porod plots from foams stabilised with 72 mM C_8TAB (circles), 29 mM $C_{10}TAB$ (triangles) and 7 mM $C_{12}TAB$ (diamonds) and 1.8 mM $C_{14}TAB$ (hexagons) in D_2O. Solid lines are fits to the paracrystalline (multilayer) model described in the text. Data have been offset for clarity. Data recorded on *D11*.

Conclusions

Foams are air-in-water colloidal systems often stabilised by small molecule surfactants or partially hydrophobic particles. Here, model “wet” foams stabilised by *surfactant(s)* have been characterised using small-angle neutron scattering to determine the nature of the surfactant layer at the interface. The SANS data showed a strong Q^{-4} dependence, with a superimposed series of inflexions over the mid Q range, whose interpretation is the subject of debate. We interpret these features within the context of a paracrystalline stack of small molecule surfactant layers. Data fitting revealed that the thickness of the stacks, L, was sensitive to the surfactant chain length, and comparable to twice the fully extended length of the hydrophobic moiety. Other parameters such as the separation of the layers, D showed minimal sensitivity to the increasing surfactant chain length and in most of the cases was estimated to be (190-175 Å). When comparing both the fitted D values and a simple calculation of the *d-spacing* from the reciprocal of the peak position, one can hypothesise that D is a term that corresponds to a defined water film between the surfactant layers. There was no obvious correlation between the interfacial structures of these surfactants and equilibrium dynamics of air-water interfaces, as characterised by film collapse or dynamic surface tension data. The insight gained in this study will assist in the rational design of surfactants used to stabilise such common systems.

References

(1) Prieto, E. M.; Page, J. M.; Harmata, A. J.; Guelcher, S. A. Injectable Foams for Regenerative Medicine. *Wiley Interdiscip. Rev. Nanomedicine Nanobiotechnology* **2014**, *6*, 136–154.

(2) Dowling, M. B.; MacIntire, I. C.; White, J. C.; Narayan, M.; Duggan, M. J.; King, D. R.; Raghavan, S. R. Sprayable Foams Based on an Amphiphilic Biopolymer for Control of Hemorrhage Without Compression. *ACS Biomater. Sci. Eng.* **2015**, *1*, 440–447.

(3) Wicklein, B.; Kocjan, A.; Salazar-Alvarez, G.; Carosio, F.; Camino, G.; Antonietti, M.; Bergström, L. Thermally Insulating and Fire-Retardant Lightweight Anisotropic Foams Based on Nanocellulose and Graphene Oxide. *Nat. Nanotechnol.* **2015**, *10*, 277–283.

(4) Bureiko, A.; Trybala, A.; Kovalchuk, N.; Starov, V. Current Applications of

Foams Formed from Mixed Surfactant-Polymer Solutions. *Adv. Colloid Interface Sci.* **2014**, *222*, 670–677.

(5) Vinogradov, A. V.; Kuprin, D. S.; Abduragimov, I. M.; Kuprin, G. N.; Serebriyakov, E.; Vinogradov, V. V. Silica Foams for Fire Prevention and Firefighting. *ACS Appl. Mater. Interfaces* **2016**, 294–301.

(6) Green, A. J.; Littlejohn, K. A.; Hooley, P.; Cox, P. W. Formation and Stability of Food Foams and Aerated Emulsions: Hydrophobins as Novel Functional Ingredients. *Curr. Opin. Colloid Interface Sci.* **2013**, *18*, 292–301.

(7) Daugelaite, D.; Guillermic, R.; Scanlon, M. G.; Page, J. H. Quantifying Liquid Drainage in Egg-White Sucrose Foams by Resistivity Measurements. *Colloids Surfaces A Physicochem. Eng. Asp.* **2016**, *489*, 241–248.

(8) Mansour, O. T.; Cattoz, B.; Heenan, R. K.; King, S. M.; Griffiths, P. C. Probing Competitive Interactions in Quaternary Formulations. *J. Colloid Interface Sci.* **2015**, *454*, 35–43.

(9) Griffiths, P. C.; Hirst, N.; Paul, A.; King, S. M. Effect of Ethanol on the Interaction between Poly (Vinylpyrrolidone) and Sodium Dodecyl Sulfate. *Langmuir* **2004**, *20*, 6904–6913.

(10) Griffiths, P. C.; Paul, A.; Stilbs, P.; Pettersson, E. Binding in Mixed Surfactant Systems. *Langmuir* **2003**, *19*, 8605–8607.

(11) Petkova, R.; Tcholakova, S.; Denkov, N. D. Role of Polymer–surfactant Interactions in Foams: Effects of pH and Surfactant Head Group for Cationic Polyvinylamine and Anionic Surfactants. *Colloids Surfaces A Physicochem. Eng. Asp.* **2013**, 1–12.

(12) Petkova, R.; Tcholakova, S.; Denkov, N. D. Foaming and Foam Stability for Mixed Polymer-Surfactant Solutions: Effects of Surfactant Type and Polymer Charge. *Langmuir* **2012**, *28*, 4996–5009.

(13) Lioumbas, J. S.; Georgiou, E.; Kostoglou, M.; Karapantsios, T. D. Foam Free Drainage and Bubbles Size for Surfactant Concentrations below the CMC. *Colloids Surfaces A Physicochem. Eng. Asp.* **2015**, *487*, 92–103.

(14) Exerowa, D. K.; Kruglyakov, P. M. *Foam and Foams Films*; Elsevier Science: Chennai, 1998.

(15) Thomas, R. K.; Penfold, J. Multilayering of Surfactant Systems at the Air-Dilute Aqueous Solution Interface. *Langmuir* **2015**, *31*, 7440–7456.

(16) Griffiths, P. C.; Paul, A.; Hirst, N. Electrophoretic NMR Studies of Polymer and Surfactant Systems. *Chem. Soc. Rev.* **2006**, *35*, 134–145.

(17) Hecht, E.; Mortensen, K. Interaction of ABA Block Copolymers with Ionic Surfactants: Influence on Micellization and Gelation. *J. Phys. Chem. B* **1995**, *88*, 4866–4874.

(18) Patel, V.; Dey, J.; Ganguly, R.; Kumar, S.; Nath, S.; Aswal, V. K.; Bahadur, P. Solubilization of Hydrophobic Alcohols in Aqueous Pluronic Solutions: Investigating the Role of Dehydration of the Micellar Core in Tuning the Restructuring and Growth of Pluronic Micelles. *Soft Matter* **2013**, *9*, 7583–7591.

(19) Alexandridis, P.; Hatton, T. A. Block Copolymer Surfactants in Aqueous Solutions and at Interface: Thermodynamics, Structure, Dynamics and Modeling. *Colloids Surfaces A Physicochem. Eng. Asp.* **1995**, *96*, 1–46.

(20) Stocco, A.; Rio, E.; Binks, B. P.; Langevin, D. Aqueous Foams Stabilized Solely by Particles. *Soft Matter* **2011**, *7*, 1260–1267.

(21) Du, Z.; Bilbao-Montoya, M. P.; Binks, B. P.; Dickinson, E.; Ettelaie, R.; Murray, B. S. Outstanding Stability of Particle-Stabilized Bubbles. *Langmuir* **2003**, *19*, 3106–3108.

(22) Howse, J. R.; Steitz, R.; Pannek, M.; Simon, P.; Schubert, D. W.; Findenegg, G. H. Adsorbed Surfactant Layers at Polymer/liquid Interfaces. A Neutron Reflectivity Study. *Phys. Chem. Chem. Phys.* **2001**, *3*, 4044–4051.

(23) Liu, X.; Dedinaite, A.; Nylander, T.; Dabkowska, A. P.; Skoda, M.; Makuska, R.; Claesson, P. M. Association of Anionic Surfactant and Physisorbed Branched Brush Layers Probed by Neutron and Optical Reflectometry. *J. Colloid Interface Sci.* **2015**, *440*, 245–252.

(24) J. Penfold, R. K. Thomas, C. C. Dong, I. Tucker, K. Metcalfe, S. Golding, and I. G. Equilibrium Surface Adsorption Behavior in Complex Anionic/Nonionic Surfactant Mixtures. *Langmuir* **2007**, *23*, 10140–10149.

(25) Xu, H.; Penfold, J.; Thomas, R. K.; Petkov, J. T.; Tucker, I.; Webster, J. R. P.; Grillo, I.; Terry, A. Ion Specific Effects in Trivalent Counterion Induced Surface

and Solution Self-Assembly of the Anionic Surfactant Sodium Polyethylene Glycol Monododecyl Ether Sulfate. *Langmuir* **2014**, *30*, 4694–4702.

(26) Halacheva, S. S.; Penfold, J.; Thomas, R. K.; Webster, J. R. P. Solution pH and Oligoamine Molecular Weight Dependence of the Transition from Monolayer to Multilayer Adsorption at the Air-Water Interface from Sodium Dodecyl Sulfate/oligoamine Mixtures. *Langmuir* **2013**, *29*, 5832–5840.

(27) Bahramian, A.; Thomas, R. K.; Penfold, J. The Adsorption Behavior of Ionic Surfactants and Their Mixtures with Nonionic Polymers and with Polyelectrolytes of Opposite Charge at the Air-Water Interface. *J. Phys. Chem. B* **2014**, *118*, 2769–2783.

(28) Fameau, A. L.; Douliez, J. P.; Boué, F.; Ott, F.; Cousin, F. Adsorption of Multilamellar Tubes with a Temperature Tunable Diameter at the Air/water Interface. *J. Colloid Interface Sci.* **2011**, *362*, 397–405.

(29) Schmidt, I.; Novales, B.; Boué, F.; Axelos, M. Foaming Properties of Protein/pectin Electrostatic Complexes and Foam Structure at Nanoscale. *J. Colloid Interface Sci.* **2010**, *345*, 316–324.

(30) Axelos, M.; Boué, F. Foams as Viewed by Small-Angle Neutron Scattering. *Langmuir* **2003**, *19*, 6598–6604.

(31) Ropers, M. H.; Novales, B.; Boué, F.; Axelos, M. Polysaccharide/Surfactant Complexes at the Air-Water Interface - Effect of the Charge Density on Interfacial and Foaming Behaviors. *Langmuir* **2008**, *24*, 12849–12857.

(32) Zhang, L.; Mikhailovskaya, A.; Yazhgur, P.; Muller, F.; Cousin, F.; Langevin, D.; Wang, N.; Salonen, A. Precipitating Sodium Dodecyl Sulfate to Create Ultrastable and Stimulable Foams. *Angew. Chemie - Int. Ed.* **2015**, *54*, 9533–9536.

(33) Curschellas, C.; Kohlbrecher, J.; Geue, T.; Fischer, P.; Schmitt, B.; Rouvet, M.; Windhab, E. J.; Limbach, H. J. Foams Stabilized by Multilamellar Polyglycerol Ester Self-Assemblies. *Langmuir* **2013**, *29*, 38–49.

(34) Micheau, C.; Bauduin, P.; Diat, O.; Faure, S. Specific Salt and pH Effects on Foam Film of a pH Sensitive Surfactant. *Langmuir* **2013**, *29*, 8472–8481.

(35) Fameau, A. L.; Saint-Jalmes, A.; Cousin, F.; Houinsou Houssou, B.; Novales,

B.; Navailles, L.; Nallet, F.; Gaillard, C.; Boué, F.; Douliez, J. P. Smart Foams: Switching Reversibly between Ultrastable and Unstable Foams. *Angew. Chemie - Int. Ed.* **2011**, *50*, 8264–8269.

(36) Ederth, T.; Thomas, R. K. A Neutron Reflectivity Study of Drainage and Stratification of AOT Foam Films. *Langmuir* **2003**, *19*, 7727–7733.

(37) Hurcom, J.; Paul, A.; Heenan, R. K.; Davies, A.; Woodman, N.; Schweins, R.; Griffiths, P. C. The Interfacial Structure of Polymeric Surfactant Stabilised Air-in-Water Foams. *Soft Matter* **2014**, *10*, 3003–3008.

(38) Rosen, M. J.; Kunjappu, J. T. *Surfactants and Interfacial Phenomena: Fourth Edition*; John Wiley and Sons: New Jersey, 2012.

(39) Holmberg, K.; Jonsson, B.; Kronberg, B.; Lindman, B. *Surfactants And Polymers In Aqueous Solutions: Second Edition*; John Wiley and Sons: Chichester, 1998; Vol. 14.

(40) Lee, J.; Nikolov, A.; Wasan, D. Foam Stability: The Importance of Film Size and the Micellar Structuring Phenomenon. *Can. J. Chem. Eng.* **2014**, *92*, 2039–2045.

(41) Etrillard, J.; Axelos, M. A. V; Cantat, I.; Artzner, F.; Renault, A.; Weiss, T.; Delannay, R. In Situ Investigations on Organic Foam Films Using Neutron and Synchrotron Radiation. *Langmuir* **2005**, *21*, 2229–2234.

(42) Zank, J.; Reynolds, P. A.; Jackson, A. J.; Baranyai, K. J.; Perriman, A. W.; Barker, J. G.; Kim, M. H.; White, J. W. Aggregation in a High Internal Phase Emulsion Observed by SANS and USANS. *Phys. B Condens. Matter* **2006**, *385–386*, 776–779.

(43) Shibayama, M.; Hashimoto, T. Small-Angle X-Ray Scattering Analyses of Lamellar Microdomains Based on a Model of One-Dimensional Paracrystal with Uniaxial Orientation. *Macromolecules* **1986**, *19*, 740–749.

(44) Kotlarchyk, M.; Ritzau, S. M. Paracrystal Model of the High-Temperature Lamellar Phase of a Ternary Microemulsion System. *J. Appl. Crystallogr.* **1991**, *24*, 753–758.